Vertical slowness constrained joint anisotropic parameters and event locations inversion for downhole microseismic monitoring

Congcong Yuan[1] and Jie Zhang[2]

[1]Department of Earth and Planetary Sciences, Harvard University, Cambridge, MA 02138, USA.
[2]School of Management, University of Science and Technology of China, Hefei, Anhui 230026, P. R. China.

Correspondence: Jie Zhang (jzhang25@ustc.edu.cn)

Abstract. The construction of accurate anisotropic velocity models plays a very important role in microseismic monitoring of hydraulic fracturing. Due to ignorance of anisotropy, severe distortions may happen in the results of microseismic location and interpretation. While the methods are existing that invert for anisotropic parameters and event locations simultaneously with microseismic traveltime, the results hinge on good velocity models and enough ray coverage for multiple parameters. Meanwhile, microseismic waveform inversion for anisotropic parameters is still challenging because of low signal-noise ratio (SNR) of the data and high computation cost. Based on the assumption of small horizontal velocity variation, we develop a method jointly inverting event locations and velocity updates using traveltimes and vertical slowness estimates. The vertical slowness estimates are independent of the source information and easy to be obtained. We apply the developed method into four synthetic examples under different circumstances. The results demonstrate that the vertical slowness can effectively constain and stabilize the conventional traveltime inversion method, in particular for the cases with the poor raypath coverage. We further employ this method for one field case where the event locations are more reasonable comparable to the inversion with traveltimes only.

1 Introduction

Including information about anisotropy is essential for the location of microseismic events during the hydraulic fracturing. For instance, in gas/oil shale cases where strong vertical transverse isotropic (VTI) anisotropy (up to 30%) is commonly seen (Warpinski et al., 2009; Eisner et al., 2009; Li et al., 2013a; Zhang et al., 2015). Due to only vertical sound speed or velocity known from the sonic logs or calibrated by perforation shots, the method becomes urgent and demanding to construct an effective anisotropic model instead of using isotropic models.

Achieving an anisotropic model is not straightforward and remains challenging for multiple parameters. Mah and Schmitt (2003) used a global search method to simultaneously determine all elastic moduli of a homogeneous composite material from travel times. However, the computer time required by their method increases very rapidly with the number of observations and unknown parameters. To obtain a velocity model that better reflects the structure between the actual microseismicity and the receivers, Grechka et al. (2011) simultaneously estimated the general anisotropy of the medium while locating the microseismicity, assuming that the medium is a homogeneous anisotropic space. However, the receiver array often spans a

large depth range and is likely to be in a very different formation from where the microseismic events are located. As a result, it could be unrealistic to assume the medium to be homogeneous in these cases. A new anisotropy velocity inversion method was then proposed by Li et al. (2013a) to determine the VTI anisotropic structure and relative event locations using the double-difference strategy with back azimuth constraint. Similarly, Han et al. (2015) simultaneously determined event locations and VTI model parameters using quasi-P and SH-waves. While the simultaneous inversion performs well in the presented cases, they are not evaluated fairly in extended cases. If velocity models, either from sonic logs (Walsh et al., 2007; Erwemi et al., 2010; Woerpel, 2010) or petrological analysis in the laboratory (Li et al., 2013b, 2014), are not sufficiently accurate, and/or coverage of raypath between event sources and receivers is poor, the trade-off between anisotropic and event parameters presents great concern (Michel and Tsvankin, 2016).

In this study, we propose incorporating phase slowness components or polarizations of quasi-P, quasi-SV, and SH waves to constrain the traditional traveltime inversion. The idea of applying the slowness or polarization method for estimating local anisotropy from vertical seismic profile (VSP) is hardly novel. Local estimation of the anisotropy parameters from traveltimes and polarizations recorded in boreholes has been conducted and discussed in a number of publications (Miller and Spencer, 1994; Horne and Leaney, 2000; Pevzner et al., 2011; Dewangan and Grechka, 2002; Grechka et al., 2007; Rusmanugroho and McMechan, 2012a, b; Tamimi et al., 2015). If the assumption of lateral homogeneity is valid, quasi-P wave slowness method is a robust method for VTI parameters (Asgharzadeh et al., 2012). Therefore, we combine the slowness method and the conventional travel time into the vertical slowness-constrained inversion method to better constrain multi-parameter inversion.

Regarding the framework of our work, we first introduce the existing traveltime inversion method and the proposed inversion method. We then apply both methods to four synthetic cases and one field case to analyze their validity upon the recovery of anisotropic model parameters and event location.

2 Methods

In this section, we introduce two inversion methods that are used for model construction and/or event locations. The first one is the currently established inversion method based on only arrival times. Inspired by the idea of the slowness method (Miller and Spencer, 1994), we further propose a joint inversion method by combining an extended slowness method as described later.

The synthetic traveltimes play an important part in the traveltime inversion. Based on the slowness method (Miller and Spencer, 1994; Kim, 1999), phase dispersion relations for qP, qSv, and SH waves can be derived from the Kelvin-Christoffel equation. If the horizontal phase slowness components P_x are given, then the vertical phase slowness components can be obtained. For quasi-P and quasi-Sv waves, the vertical slowness components are expressed as,

$$P_z^{qP} = \sqrt{\frac{B - \sqrt{B^2 - 4C}}{2}}. \tag{1}$$

$$P_z^{qSv} = -\sqrt{\frac{B - \sqrt{B^2 - 4C}}{2}}. \tag{2}$$

Where,

$$B = \frac{1}{\alpha_0^2} + \frac{1}{\beta_0^2} - 2\left(1 + \delta + (\epsilon - \delta)\frac{\alpha_0^2}{\beta_0^2}\right)P_x^2, \tag{3}$$

$$C = \left((1 + 2\epsilon)P_x^2 - \frac{1}{\alpha_0^2}\right)\left(P_x^2 - \frac{1}{\beta_0^2}\right). \tag{4}$$

For the SH wave, the vertical slowness components are expressed as,

$$P_z^{SH} = \sqrt{\frac{1}{\beta_0^2} - (1 + 2\gamma)P_x^2}. \tag{5}$$

where P_Z^{qP}, P_Z^{qSv}, and P_Z^{SH} are the vertical slowness components of quasi-P and quasi-Sv and SH waves, respectively. α_0, β_0, ϵ, δ, and $gamma$ are the Thomsen's parameters defined by Thomsen (1986). Then based on the relations of slowness components and group velocities, the traveltime can be calculated. Here, we synthesize the traveltimes with the shooting algorithm by trying different P_X (Han et al., 2015).

2.1 Traveltime inversion method (TM)

In microseismic data processing, the observed arrival time T_{ij} from a microseismic event i to a receiver j installed in the well is formulated as,

$$T_{ij} = \tau_i + t_{ij}, \tag{6}$$

$$t_{ij} = \int_{\text{raypath}} \frac{1}{V_g}\, dl. \tag{7}$$

Where T_{ij} is the arrival time. τ_i is the origin time of the event i. t_{ij} is the traveltime from a microseismic event i to a receiver j. V_g is the group velocity structure. dl is an element of raypath length. The event location, origin time, and group velocity structure are the unknowns. The traveltimes can be synthetized by the raytracing method of the shooting algorithm that based on the slowness components (Cervenỳ, 2001; Tang and Li, 2008; Han et al., 2015).

Based on the prior information, the linear approximation of the arrival time residuals can be expressed to the perturbations of the event and group velocity model parameters,

$$\Delta T_{ij} = T_{ij}^{\text{obs}} - T_{ij}^{\text{syn}} = \Delta\tau_i + \sum_{k=1}^{3} \frac{\partial T_{ij}}{\partial x_k}\Delta x_k + \sum_{l=1}^{\text{raypath}} \frac{\partial T_{ij}}{\partial V_g^l}\Delta V_g^l. \tag{8}$$

where T_{ij}^{obs} is the observed arrival time data. T_{ij}^{syn} represents the synthetic arrival time data based on the prior information. $\Delta\tau$ is the origin time perturbation. Δx stands for the event location perturbation.

According to the relations between the group velocity and Thomsen's parameters (Thomsen, 1986; Kim, 1999; Han et al., 2017), we can transform the equation (8) into the following equations. For quasi-P wave, the above equation can be re-written as,

$$\Delta T_{ij}^{qP} = \Delta\tau_i + \sum_{k=1}^{3} \frac{\partial T_{ij}^{qP}}{\partial x_k}\Delta x_k + \sum_{l=1}^{\text{raypath}} \frac{\partial T_{ij}^{qP}}{\partial \alpha_0^l}\Delta\alpha_0^l + \sum_{l=1}^{\text{raypath}} \frac{\partial T_{ij}^{qP}}{\partial \beta_0^l}\Delta\beta_0^l + \sum_{l=1}^{\text{raypath}} \frac{\partial T_{ij}^{qP}}{\partial \epsilon^l}\Delta\epsilon^l + \sum_{l=1}^{\text{raypath}} \frac{\partial T_{ij}^{qP}}{\partial \delta^l}\Delta\delta^l. \tag{9}$$

For the quasi-Sv wave, the equation (8) can be re-written as,

$$\Delta T_{ij}^{qSv} = \Delta\tau_i + \sum_{k=1}^{3} \frac{\partial T_{ij}^{qSv}}{\partial x_k}\Delta x_k + \sum_{l=1}^{\text{raypath}} \frac{\partial T_{ij}^{qSv}}{\partial \alpha_0^l}\Delta\alpha_0^l + \sum_{l=1}^{\text{raypath}} \frac{\partial T_{ij}^{qSv}}{\partial \beta_0^l}\Delta\beta_0^l + \sum_{l=1}^{\text{raypath}} \frac{\partial T_{ij}^{qSv}}{\partial \epsilon^l}\Delta\epsilon^l + \sum_{l=1}^{\text{raypath}} \frac{\partial T_{ij}^{qSv}}{\partial \delta^l}\Delta\delta^l. \tag{10}$$

For the SH wave, the equation (8) can be re-written as,

$$\Delta T_{ij}^{SH} = \Delta\tau_i + \sum_{k=1}^{3} \frac{\partial T_{ij}^{SH}}{\partial x_k}\Delta x_k + \sum_{l=1}^{\text{raypath}} \frac{\partial T_{ij}^{SH}}{\partial \beta_0^l}\Delta\beta_0^l + \sum_{l=1}^{\text{raypath}} \frac{\partial T_{ij}^{SH}}{\partial \gamma^l}\Delta\gamma^l. \tag{11}$$

where $\Delta\alpha_0$, $\Delta\beta_0$, $\Delta\epsilon_0$, and $\Delta\gamma_0$ are the perturbations of the arrival time to the Thomsen's parameters. To express simply, we include all the Thomsen's parameters into the model vector m. Due to the complexity of detecting arrival time for quasi-SV wave, and the multi-value of quasi-SV group velocities, we are difficult to adopt the traveltime information of quasi-SV wave in reality, although we can compute the quasi-SV traveltimes in means of shortest raypath method by avoiding shadow zone (Han et al., 2015). Hence, only quasi-P and SH traveltimes are utilized in this study and the scheme adopted for the inversion for event locations and velocity model is therefore constructed as,

$$\begin{bmatrix} 1 & W_m^{qP}A_m^{qP} & W_x^{qP}A_x^{qP} \\ 1 & W_m^{SH}A_m^{SH} & W_x^{SH}A_x^{SH} \end{bmatrix} \begin{bmatrix} \Delta t_0 \\ \Delta m/W_m \\ \Delta x/W_x \end{bmatrix} = \begin{bmatrix} T_{\text{obs}}^{qP} - T_{\text{syn}}^{qP} - T_0^{qP} \\ T_{\text{obs}}^{SH} - T_{\text{syn}}^{SH} - T_0^{SH} \end{bmatrix}. \tag{12}$$

where A_m and A_x are the derivatives of traveltime with respect to Thomsen parameters and event locations, respectively. Δm, Δt_0, and Δx represent the perturbations to Thomsen parameters, origin time, and event location, respectively. T_{obs}^P and T_{obs}^{SH} are the observed arrival times of quasi-P and SH waves, respectively. T_{syn}^P and T_{syn}^{SH} mean the synthetic arrival times of quasi-P and SH waves, respectively. The initial values will be set before the inversion, then in every iteration the values will be updated. In order to reduce the influence of different magnitude of Thomsen parameters and event locations, the weighting

values W_x and W_m would be added in the inversion. We test a lot of weighting values and find that it can improve the inverted results to set W_x equals to 1000 and W_m with respect to ϵ, δ, and γ equal to 1000. If W_x equals to zero, the inversion is adopted to invert for only model parameters and the event location remains unchanged.

The non-linear inversion has a strong dependence on initial models. Under most circumstances, because of severe nonlinearity and trade-off, numerical iterations are needed but still cannot address the problems, the test results will be shown in the later testing section. Thus, the slowness components of the VSP data are suggested to use and constrain the traveltime-based inversion.

2.1.1 Vertical slowness constrained traveltime inversion method (VTM)

VSP surveys with multicomponent geophones provide a unique opportunity to measure the slowness components or polarization vectors. These measurements are employed in the inversion for the elements of the stiffness tensors, or the equivalent anisotropy parameters (Grechka et al., 2011; Tamimi et al., 2015). Although we can use polarization measurements, Asgharzadeh et al. (2012) suggested that for lateral homogeneous formation the slowness method is more accurate.

Similar to the equations (5), the linear approximation of the vertical phase slowness components can be expressed to the perturbations of the group velocity model parameters. For quasi-P wave, the linearized expression can be written as,

$$\Delta P_z^{qP} = \sum_{l=1}^{\text{raypath}} \left(\frac{\partial P_z^{qP}}{\partial \alpha_0^l} \Delta \alpha_0^l + \frac{\partial P_z^{qP}}{\partial \beta_0^l} \Delta \beta_0^l + \frac{\partial P_z^{qP}}{\partial \epsilon^l} \Delta \epsilon^l + \frac{\partial P_z^{qP}}{\partial \delta^l} \Delta \delta^l \right). \tag{13}$$

For the quasi-Sv wave, the linearized expression can be written as,

$$\Delta P_z^{qSv} = \sum_{l=1}^{\text{raypath}} \left(\frac{\partial P_z^{qSv}}{\partial \alpha_0^l} \Delta \alpha_0^l + \frac{\partial P_z^{qSv}}{\partial \beta_0^l} \Delta \beta_0^l + \frac{\partial P_z^{qSv}}{\partial \epsilon^l} \Delta \epsilon^l + \frac{\partial P_z^{qSv}}{\partial \delta^l} \Delta \delta^l \right). \tag{14}$$

For the SH wave, the linearized expression can be written as,

$$\Delta P_z^{SH} = \sum_{l=1}^{\text{raypath}} \left(\frac{\partial P_z^{SH}}{\partial \beta_0^l} \Delta \beta_0^l + \frac{\partial P_z^{SH}}{\partial \gamma^l} \Delta \gamma^l \right). \tag{15}$$

where Δ_{P_z} is the difference of theoretical and real vertical phase slowness components. The real components can be obtained by the adjacent receivers. We can extract the high-resolution arrival time difference between two receivers by cross-correlating their recordings. Then the vertical slowness components can be approximately calculated by the arrival time difference dividing with their distance (Miller and Spencer, 1994), which is expressed as equation (17). From the above equations, we can find that the slowness components do not depend on the source parameters. Hence, we can extend the active source gather (Miller and Spencer, 1994) to the common passive source gather (see Figure 1a), the source can be a perforation shot or microseismic event with unknown source information. Based on the above equations, the local anisotropic parameters can be effectively derived (Asgharzadeh et al., 2012). Such low-cost measurements can be applied to constrain the traveltime inversion. Therefore, we further develop equation (12) by incorporating the slowness estimates as follows,

$$\begin{bmatrix} 1 & W_m^{qP} A_{T,m}^{qP} & W_x^{qP} A_x^{qP} \\ 1 & W_m^{SH} A_{T,m}^{SH} & W_x^{SH} A_x^{SH} \\ 0 & W_m^{qP} A_{Pz,m}^{qP} & 0 \\ 0 & W_m^{SH} A_{Pz,m}^{SH} & 0 \end{bmatrix} \begin{bmatrix} \Delta t_0 \\ \Delta m/W_m \\ \Delta x/W_x \end{bmatrix} = \begin{bmatrix} T_{\text{obs}}^{qP} - T_{\text{syn}}^{qP} - T_0^{qP} \\ T_{\text{obs}}^{SH} - T_{\text{syn}}^{SH} - T_0^{SH} \\ P_{Z,\text{obs}}^{qP} - P_{Z,\text{syn}}^{qP} \\ P_{Z,\text{obs}}^{SH} - P_{Z,\text{syn}}^{SH} \end{bmatrix}, \tag{16}$$

$$P_Z \approx \frac{T_{i,k} - T_{j,k}}{d_{ij}}. \tag{17}$$

In this joint inversion, we add a weighting scale to balance the arrival times and the vertical phase slowness components. The weighting value depends on the variation of the horizontal layer. If the layer could not be regarded as the homogeneous formation, we set the weighting to a small value. Additionally, in our inversion, only when two and two more receivers in the same layer, they can be utilized to calculate the vertical phase slowness components. If one layer contains no receivers or only one receiver, then the parameters of the layer will be not constrained in the above inversion. Hence, more receivers deployed in the same layer, better the layer's parameters are constrained; meanwhile, if the receivers can span more layers, the inversion can constrain the inversion better.

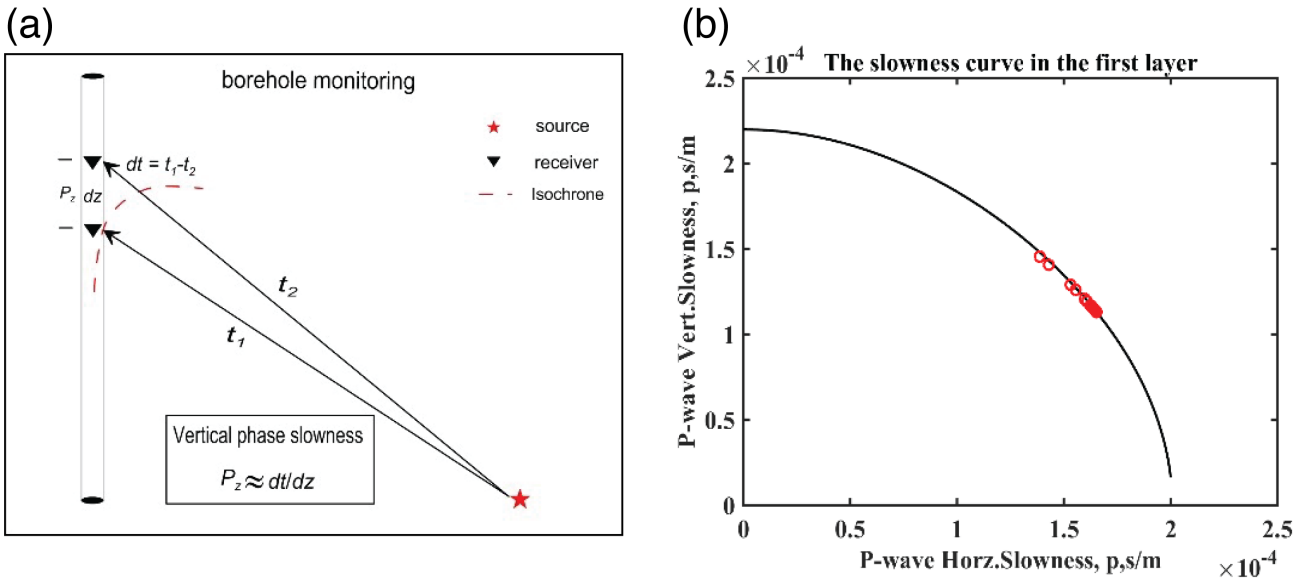

Figure 1. (a) the diagram of the slowness method; (b) the projection of the vertical slowness estimated using two receivers in the first layer of the velocity model on the theoretical slowness surface. The red circles are from the ten samples at a depth of 2000 m of the velocity model as shown in Figure 2a.

3 Numerical examples

We construct a realistic VTI layer model illustrated as Figure 2a), which contains eight layers with one low-velocity thin layer in the range from 1700 m to 2200 m. To verify the validity of the vertical slowness estimations, in the model we randomly select 10 positions at the depth of 2 km. Provided with ten horizontal slowness, ten vertical slowness components are derived using the arrival time residual and the distance of two adjacent receivers in the first layer. As shown in Figure 1a, the vertical slowness component is approximately calculated by the traveltime residual and distance of two neighboring receivers. Then we project ten slowness components on the theoretical slowness surface obtained from the Christoffel equation. Figure 1b illustrates that these values are consistent with the theoretical values, which means that these data are effective to be used to derive the model parameters.

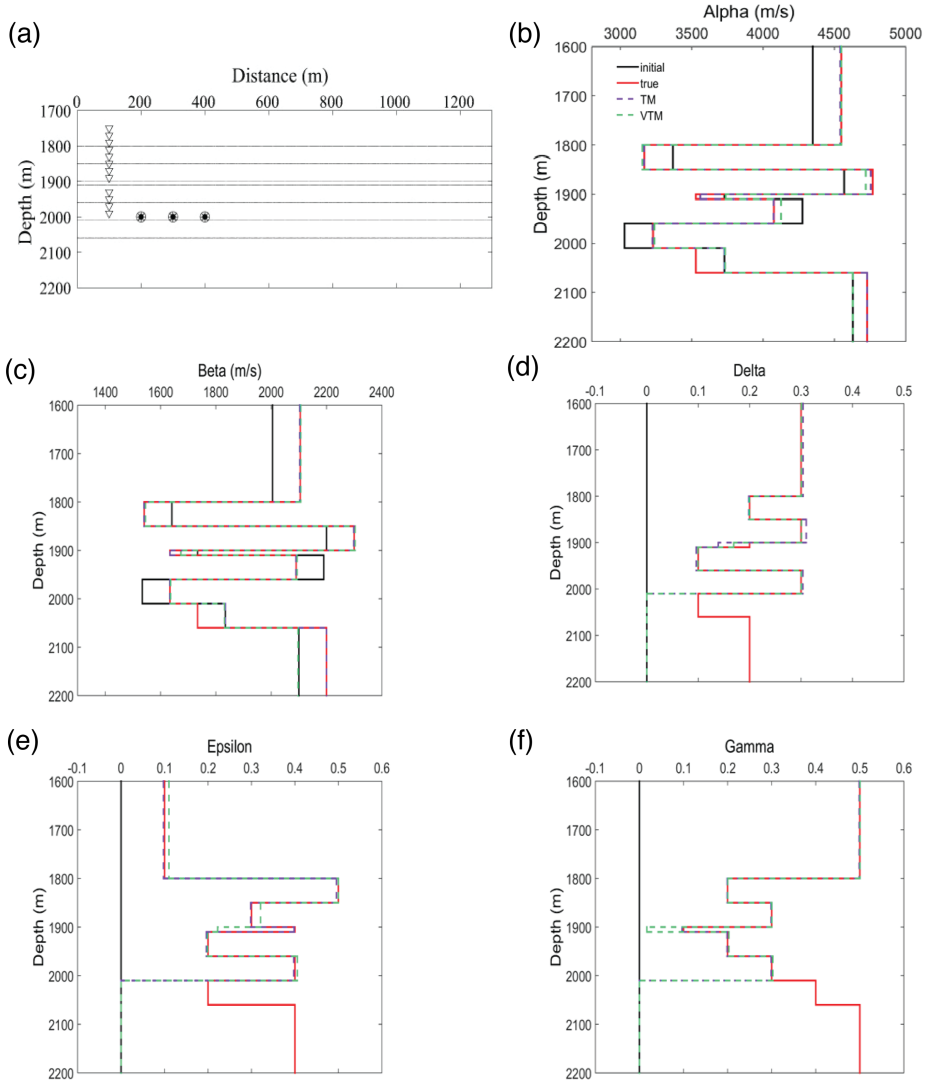

Figure 2. The survey geometry and inverted model results for the case 1. (a) The velocity model includes eight layers from depth of 1700 m to 2200 m. Twelve receivers in several layers are marked by triangles. Three circles represent perforations or drop-balls at known positions. Case 1 is an example with three near-offset perforations or drop-balls. (b-f) The five velocity solutions are derived by two methods. The black, red, purple, and green lines included stand for initial, true, and inverted parameters by TM and VTM, respectively.

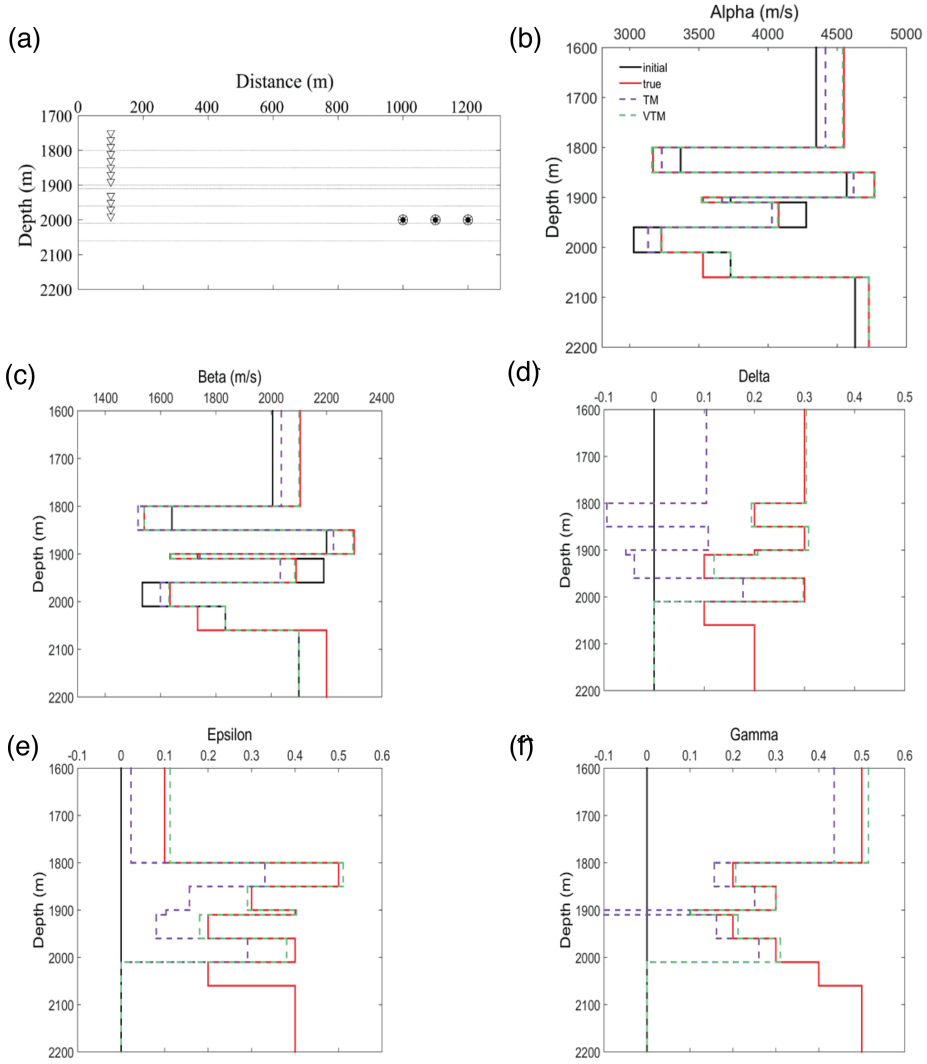

Figure 3. The survey geometry and inverted model results of case 2. (a) The model includes eight layers from depth of 1700 m to 2200 m. Twelve receivers are marked by triangles, which are distributed in different layers. The three circles, black dots, and stars represent perforations or drop-balls with known positions (they are fixed). Case 2 is the example with three far-offset perforations or drop-balls. (b-f) The five velocity solutions are derived by two methods. The black, red, purple, and green lines included stand for initial, true, and inverted parameters by TM and VTM, respectively.

To validate the efficiency of our method, we conduct four synthetic tests in our study. In the first two cases, the location is not considered in the inversion, that is, the inversion is only applied to yield model parameters and unknown origin time. In another two cases, we consider both source and model parameters in the inversion. Starting from the case one, we place three perforation shots nearby the receiver array as seen in Figure 2a. In the inversion, we assume that the locations of perforation shots are known, but their origin times remain unknown. And only two among five initial anisotropic parameters α_0 and β_0,

can be obtained by sonic logs, while the other three initial models are set to zero. These model parameters are then calibrated by perforation shots using TM and VTM. Only traveltime data are used for the TM inversion, and the data from both traveltime and vertical slowness components are input into the VTM. Note that only the layers with at least two receivers could be uitilized to estimate vertical slowness components to constrain model parameters of the layer. The inversion results (Figure 2b-f) show that almost all parameters are recovered well. In this case, the ray coverage is enough for the TM so that the inversion is not trapped in the local minimum and produces satisfactory results.

To test whether raypath coverage has an effect on the inversion, we shift the perforation shots to the right a lot (see Figure 3a). In case two, the models conducted are the same as in case one. The only difference is the positions of the perforation shots. In Figure 3b-f, the comparison of these inverted results using two different methods shows that VTM could still result in stable results with the aid of the vertical slowness constraint, while TM could not recover the model parameters only using the traveltime information.

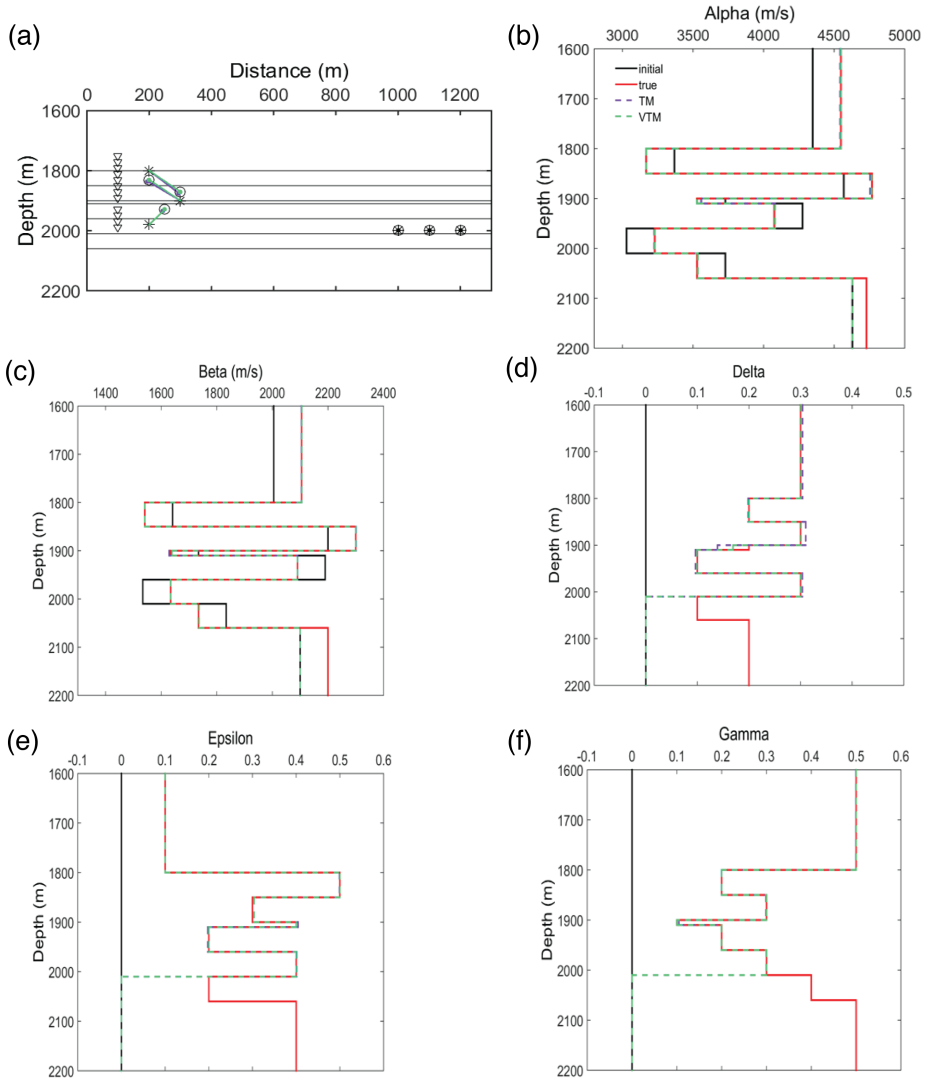

Figure 4. The survey geometry and inverted model results of case 3. (a) In the model the reverse triangles are the receivers, the perforation shots are marked by red rectangle and three stars, circles, and dots present the initial, true, and inverted locations, respectively. The purple and green represent TM and VTM method, respectively. (b-f) The inverted model results of case 3. The black, red, purple, and green lines included stand for initial, true, and inverted parameters by TM and VTM, respectively.

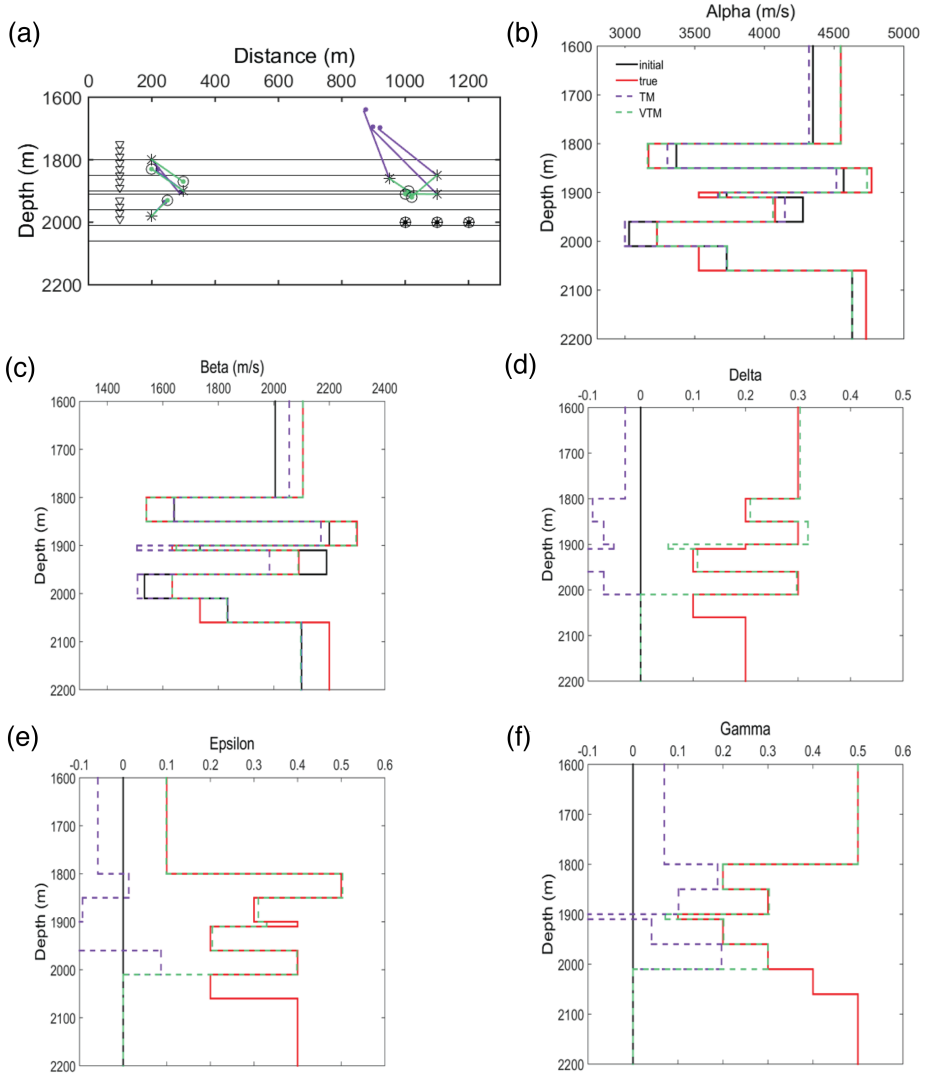

Figure 5. The survey geometry and inverted model results of case 4. (a) In the model the reverse triangles are the receivers, the perforation shots are marked by red rectangle and three stars, circles, and dots present the initial, true, and inverted locations, respectively. The purple and green represent TM and VTM method, respectively. (b-f) The inverted model results of case 4. The black, red, purple, and green lines included stand for initial, true, and inverted parameters by TM and VTM, respectively.

In some cases, if we only calibrate the model parameters by the perforation, it may cause velocity-related errors in locating the microseismic events, where the ray trajectories of the perforation shots do not cover (Grechka, 2010). Hence, we add three near-offset events into the case 3. In this case (Figure 4a), the model parameters as well as three near-offset events are inverted simultaneously. The results of case three (Figure 4b-f) illustrate that the location and model parameters are inverted well using

both TM and VTM, because the added near-receiver events lead to a better raypath coverage. The VTM is also effective for the event location and model parameters recovery.

If we add another three far-offset events into the case three, the location results (Figure 5a) demonstrate that, for the locations results (marked by the purple color) of the TM, the near-offset event locations are better than the far-offset locations, but they all deviate from the true locations. Fortunately, the locations results of VTM demonstrate that all the event locations could be inverted well. Figure 5b-f illustrates that the VTM is more effective to recover the model parameters than the TM. Accordingly, once events with poor raypath coverage are input in the inversion, the results are challenging to reconstruct well. Nevertheless, in the VTM the vertical slowness components could provide another constraint upon the traveltime inversion and make the inversion stable. In all synthetic cases, the raypaths cover the first six layers from the sources to the receivers, hence only the top six layers are updated in the inversion results. Additionally, in the fourth layer, due to its small thickness, the layer could not obtain an effective ray coverage, and vertical slowness components are not measured in that layer. Therefore, the Thomsen's parameters of the thin layer are not recovered well in both TM and VTM inversions.

4 One field example

We further apply two methods to a real data set, which is acquired from a single vertical monitoring well during a hydraulic fracturing treatment. Microseismic data were recorded during 12 stages of hydraulic fracturing. Twelve three-component receivers were deployed in a vertical monitoring well from 2070 m to 2415m depth, with a receiver interval of 15 m (Figure 6). Within each stage, a ball-drop event was recorded with known location but an unknown origin time. Each ball-drop could trigger many microseismic events, which are mainly happened nearby the ball-drop. In addition, the sonic logging data could provide a 1D velocity model but merely contain vertical P- and S-wave velocities. Under this circumstance, the vertical P- and S-wave velocities are regarded as the initial velocities in the inversion and other model parameters are all set to zero.

Here, we do not calibrate the model parameters using dropballs at first, because the number of effective dropballs is limited. We select 37 events of stage 3 as well as 32 events of stage 4 for the processing. Arrivals of their P and S waves are picked up manually. Upon archiving arrival times, the vertical slowness data could be derived approximately by using equation (17). With all these measured data, we apply TM and VTM to invert the event locations and model parameters, respectively. Meanwhile, all events are first located in a 2D profile and then projected to 3D by event azimuths from a separate analysis of the calibrated P-wave polarizations.

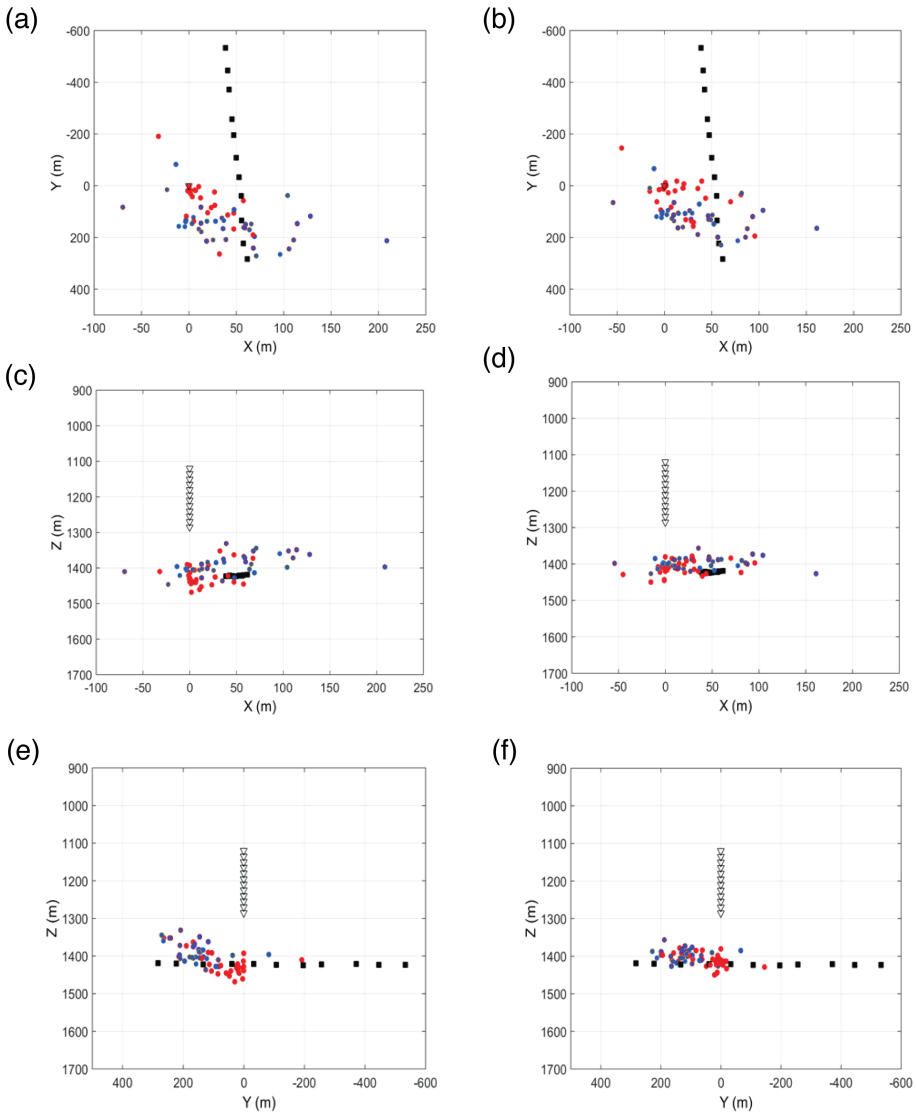

Figure 6. The different projections of event location results. The left maps (a, c, e) show the projections of locations on X-Y, X-Z, and Y-Z using the TM, and the right ones (b, d, f) are the projections of locations on X-Y, X-Z, and Y-Z using the VTM. The triangle array represents receiver array, the black squares are ball-drops. The red dots are the event location results of stage 3, the blue ones are the event location results of stage 4.

190 In the projections of location results (Figure 6), the event locations obtained with the VTM are more convergent than the location results of TM, especially in the area marked by the green ellipse. Additionally, the X-Z projection shows that the results of the two stages are obviously more separated in VTM locations than in TM locations. Hence, the VTM locations are more reasonable compared to the TM ones. This may be attributed to the vertical slowness components that provide an additional constraint on the inversion process. In addition, the model results (Figure 7) with both inversion methods reveal

weak anisotropy in the field situation, which can be observed in the recordings of the receiver array. Although we could not further verify the results in the field or with other supportive data, the above theoretical analysis and numerical examples help us understand the differences in the results of the two methods.

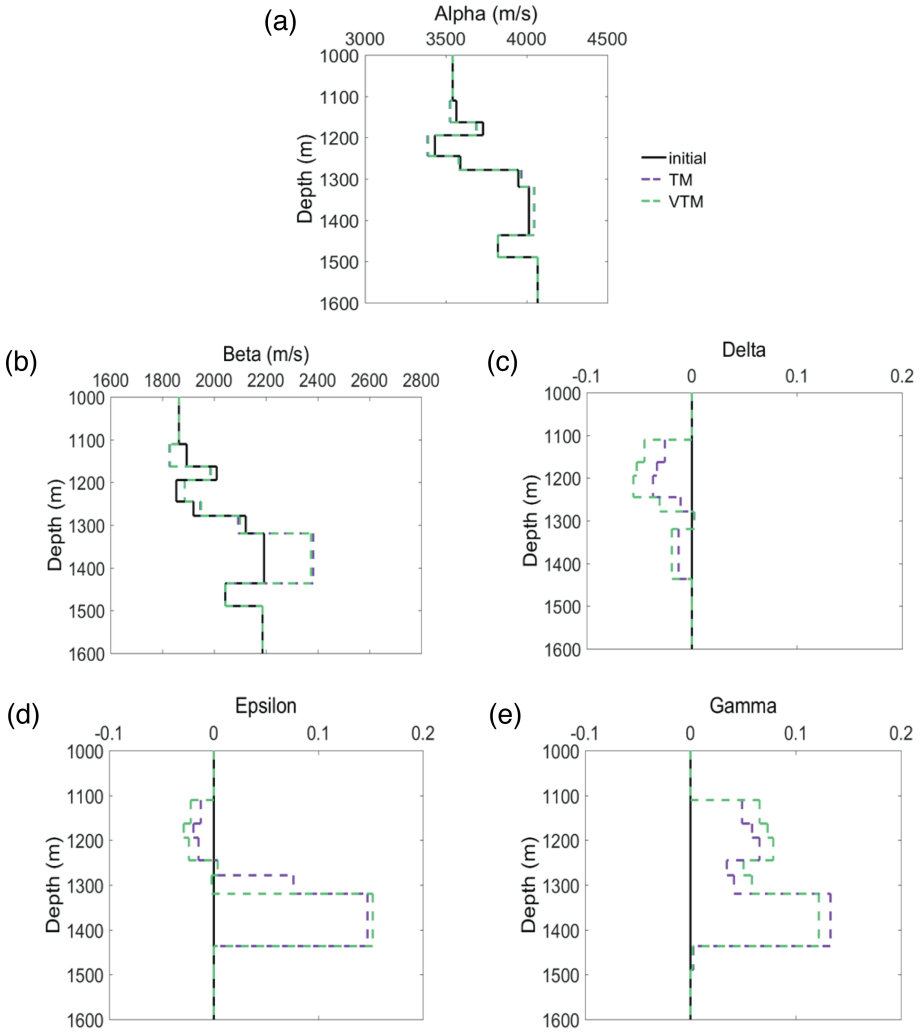

Figure 7. The inverted model results of the real case. (a-e) the five velocity solutions are derived by two methods. The black, red, purple, and green lines included stand for initial, true, and inverted parameters by TM and VTM, respectively.

5 Conclusions

In this study, we introduce a new inversion scheme that integrates vertical slowness components with traveltime inversion to extract VTI parameters and pinpoint event locations simultaneously or to refine the velocity model alone. Our approach, com-

pared to traditional methods that rely solely on traveltime inversion, exhibits greater stability, particularly in scenarios with inadequate raypath coverage. In our initial two synthetic examples, we focus exclusively on inverting for model parameters and original times without attempting to locate the event positions. The results confirm that our method (VTM) consistently outperforms traditional traveltime methods (TM), regardless of raypath coverage sufficiency. In the subsequent two synthetic cases, we simultaneously invert for both the event locations and model parameters. These examples demonstrate that incorporating vertical slowness enhances the inversion's ability to constrain both the event locations and model parameters effectively. Field applications reveal that the VTM method enhances the accuracy of event locations due to the incorporation of the vertical slowness. In practice, the deeper event locations relative to the borehole are suggested to utilize, because the approximation of vertical slowness becomes more precise at greater depths. Besides, the slowness method's effectiveness diminishes in formations with substantial horizontal velocity variations, where the slowness-polarization approach might be more suitable.

Author contributions. Authors contributions: C.Y.: methodology, software, validation, formal analysis, investigation, writing, visualization; J.Z.: writing, formal analysis, project administration, funding acquisition.

Competing interests. The authors declare that they have no conflict of interests.

Acknowledgements. We appreciate the support from GeoTomo, allowing us to use MiVu software package to perform this study.

References

Asgharzadeh, M., Bona, A., Pevzner, R., Urosevic, M., and Gurevich, B.: Uncertainties in local anisotropy estimation from multi-offset VSP data, in: 74th EAGE Conference and Exhibition incorporating EUROPEC 2012, pp. cp–293, European Association of Geoscientists & Engineers, 2012.

Cervenỳ, V.: Seismic ray theory, vol. 110, Cambridge university press Cambridge, 2001.

Dewangan, P. and Grechka, V.: Inversion of multi-component, multi-azimuth, walkaway VSP data for the stiffness tensor, in: SEG Technical Program Expanded Abstracts 2002, pp. 161–164, Society of Exploration Geophysicists, 2002.

Eisner, L., Duncan, P. M., Heigl, W. M., and Keller, W. R.: Uncertainties in passive seismic monitoring, The Leading Edge, 28, 648–655, 2009.

Erwemi, A., Walsh, J., Bennett, L., Woerpel, C., and Purcell, D.: Anisotropic velocity modeling for microseismic processing: part 3-borehole sonic calibration case study, in: SEG International Exposition and Annual Meeting, pp. SEG–2010, SEG, 2010.

Grechka, V.: Data-acquisition design for microseismic monitoring, The Leading Edge, 29, 278–282, 2010.

Grechka, V., Mateeva, A., Gentry, C., Jorgensen, P., Lopez, J., and Franco, G.: Estimation of seismic anisotropy from P-wave VSP data, The Leading Edge, 26, 756–759, 2007.

Grechka, V., Singh, P., and Das, I.: Estimation of effective anisotropy simultaneously with locations of microseismic events, Geophysics, 76, WC143–WC155, 2011.

Han, S., Zhang, W., and Zhang, J.: Joint microseismic quasi-P and SH traveltime inversion for updating VTI parameters, in: SEG International Exposition and Annual Meeting, pp. SEG–2015, SEG, 2015.

Han, S., Zhang, W., and Zhang, J.: Calculating qP-wave traveltimes in 2-D TTI media by high-order fast sweeping methods with a numerical quartic equation solver, Geophysical Journal International, 210, 1560–1569, 2017.

Horne, S. and Leaney, S.: Short note: Polarization and slowness component inversion for TI anisotropy., Geophysical Prospecting, 48, 2000.

Kim, S.: On eikonal solvers for anisotropic traveltimes, in: SEG Technical Program Expanded Abstracts 1999, pp. 1875–1878, Society of Exploration Geophysicists, 1999.

Li, J., Zhang, H., Rodi, W. L., and Toksoz, M. N.: Joint microseismic location and anisotropic tomography using differential arrival times and differential backazimuths, Geophysical Journal International, 195, 1917–1931, 2013a.

Li, J., Li, C., Morton, S. A., Dohmen, T., Katahara, K., and Nafi Toksöz, M.: Microseismic joint location and anisotropic velocity inversion for hydraulic fracturing in a tight Bakken reservoir, Geophysics, 79, C111–C122, 2014.

Li, J. et al.: Study of induced seismicity for reservoir characterization, Ph.D. thesis, Massachusetts Institute of Technology, 2013b.

Mah, M. and Schmitt, D. R.: Determination of the complete elastic stiffnesses from ultrasonic phase velocity measurements, Journal of Geophysical Research: Solid Earth, 108, ECV–6, 2003.

Michel, O. J. and Tsvankin, I.: Anisotropic waveform inversion for microseismic velocity analysis and event location, in: SEG International Exposition and Annual Meeting, pp. SEG–2016, SEG, 2016.

Miller, D. E. and Spencer, C.: An exact inversion for anisotropic moduli from phase slowness data, Journal of Geophysical Research: Solid Earth, 99, 21 651–21 657, 1994.

Pevzner, R., Gurevich, B., and Urosevic, M.: Estimation of azimuthal anisotropy from VSP data using multicomponent S-wave velocity analysis, Geophysics, 76, D1–D9, 2011.

Rusmanugroho, H. and McMechan, G. A.: 3D, 9C seismic modeling and inversion of Weyburn Field data, Geophysics, 77, R161–R173, 2012a.

Rusmanugroho, H. and McMechan, G. A.: Sensitivity of estimated elastic moduli to completeness of wave type, measurement type, and illumination apertures at a receiver in multicomponent VSP data, Geophysics, 77, R1–R18, 2012b.

Tamimi, N., Tsvankin, I., and Davis, T. L.: RSTIMATION OF VTI PARAMETERS USING SLOVVNESS-POLARIZATION INVERSION OF P. AND SV-VVAVES, Journal of seismic exploration, 24, 455–474, 2015.

Tang, W. and Li, L.: Exact traveltime computation in multi-layered transversely isotropic media with vertical symmetry axis, Acta Seismologica Sinica, 21, 370–379, 2008.

Thomsen, L.: Weak elastic anisotropy, Geophysics, 51, 1954–1966, 1986.

Walsh, J., Sinha, B., Plona, T., and Ammerman, M.: Derivation of anisotropy parameters in a shale using borehole sonic data, in: SEG International Exposition and Annual Meeting, pp. SEG–2007, SEG, 2007.

Warpinski, N. R., Waltman, C. K., Du, J., and Ma, Q.: Anisotropy effects in microseismic monitoring, in: SPE Annual Technical Conference and Exhibition?, pp. SPE–124 208, SPE, 2009.

Woerpel, C.: Anisotropic velocity modeling for microseismic processing: Part 2—Fast and accurate model calibration with a cross-well source, in: SEG Technical Program Expanded Abstracts 2010, pp. 2135–2139, Society of Exploration Geophysicists, 2010.

Zhang, J., Liu, H., Zou, Z., and Huang, Z.: Velocity modeling and inversion techniques for locating microseismic events in unconventional reservoirs, Journal of Earth Science, 26, 495–501, 2015.